Four-point Cluster application of magnetic field analysis tools: The Curlometer

M. W. Dunlop, A. Balogh, K. -H. Glassmeier, P. Robert

JOURNAL OF GEOPHYSICAL RESEARCH, VOL. 107, NO. A11, 1384, doi:10.1029/2001JA005088, 2002

Four-point Cluster application of magnetic field analysis tools: The Curlometer

M. W. Dunlop[1] and A. Balogh
Space and Atmospheric Physics Group, Imperial College, London, UK

K.-H. Glassmeier
Institut für Geophysik und Meteorologie, Technische Universitat Braunschweig, Braunschweig, Germany

P. Robert
Centre d'Etude des Environnements Terrestre et Planétaires/IPSL, Velizy, France

Received 24 September 2001; revised 1 February 2002; accepted 18 March 2002; published 20 November 2002.

[1] For the first time, the Cluster spacecraft have collected 3-D information on magnetic field structures at small to medium scales in the Earth's dayside magnetosphere. We focus here on the first application of the Curlometer (direct estimation of the electric current density from *curl*(***B***), using measured spatial gradients of the magnetic field) analysis technique. The applicability of this multipoint technique is tested, for selected events within the data set, in the context of various mission constraints (such as position, timing, and experimental accuracy). For the Curlometer, nonconstant spatial gradients over the spacecraft volume, time dependence, and measurement errors can degrade the quality of the estimate. The estimated divergence of the magnetic field can be used to monitor (indirectly) the effect of nonconstant gradients in the case of many magnetic field structures. For others, and at highly distorted spacecraft configurations, this test may not reflect the quality of the Curlometer well. The relative scales and relative geometry between the spacecraft array and the structures present, as well as measurement errors, all are critical to the quality of the calculation. We demonstrate that even when instrumental and other errors are known to contribute to the uncertainty in the estimate of the current, a number of current signatures within the magnetosphere can be plausibly determined in direction, if not absolute size. A number of examples show consistent currents at the magnetopause, both separate from, and nearby or in the cusp region. Field-aligned currents near the polar cap boundary are also estimated reliably. We also demonstrate one example of an anomalous current arising from the effect of a highly distorted spacecraft configuration. *INDEX TERMS:* 2708 Magnetospheric Physics: Current systems (2409); 2724 Magnetospheric Physics: Magnetopause, cusp, and boundary layers; 2794 Magnetospheric Physics: Instruments and techniques; *KEYWORDS:* electric current vector, multispacecraft technique

Citation: Dunlop, M. W., A. Balogh, K.-H. Glassmeier, and P. Robert, Four-point Cluster application of magnetic field analysis tools: The Curlometer, *J. Geophys. Res.*, *107*(A11), 1384, doi:10.1029/2001JA005088, 2002.

1. Introduction

[2] The four-spacecraft array of Cluster spacecraft is providing an unprecedented data set of coordinated multipoint measurements and has now covered the whole of the duskside magnetosphere. The fluxgate magnetometer experiment, in particular, is providing high time resolution (22.4 and 67 Hz) magnetic field measurements from all four spacecraft [*Balogh et al.*, 2001]. This data set has allowed the first tests of long envisaged, four-spacecraft, magnetic field analysis techniques [see, e.g., *Dunlop et al.*, 1988, 1990; *Robert and Roux*, 1990; *Neubauer and Glassmeier*, 1990] to be carried out with actual measurements. Cluster is unique in maintaining an array of closely separated spacecraft every orbit (~600 km at the time of the measurements reported here). The four spacecraft are in a mean geopolar, eccentric ($4 \times 19.6\ R_E$), orbit, each with identical orbital periods (apart from minor perturbations), but with slightly different orbital elements. At any time, the configuration of spacecraft can be represented by the set of spacecraft separation vectors, which give their instantaneous relative positions. The shape and orientation of this spatial configuration varies widely as the spacecraft proceed along the

[1]Now at Space Sciences Division, Space Science and Technology Department, Rutherford Appleton Laboratory, Chilton, UK.

0148-0227/02/2001JA005088

orbit (as a result of Keplerian evolution). In order to set an overall scale for the configuration, however, manoeuvres are performed at intervals during the mission.

[3] Many multispacecraft analysis techniques need particular application to the Cluster data. Indeed, the properties of interest are as significant as the spacecraft configuration when considering how the analysis may be applied, and the quality of any analysis is critically limited by measurement uncertainty. The use of a multispacecraft technique must therefore be event dependent. The configuration can sample the magnetic field behavior in very different ways at different positions along the orbit (see for example Figure 4). This has the consequence that some combinations of the four-point measurements will be more fruitful than others will be, hence some techniques will be better suited than others. Nevertheless, much of the anisotropic structure in the magnetosphere can be described by similar global frames of reference. For example, known magnetosheath phenomena tend to be ordered by a boundary, flow and field-aligned system [*Dunlop et al.*, 1993] so that often Cluster configurations can be well matched to these natural coordinates. As well as these spatial considerations, the direct separation of temporal and spatial variations with Cluster is not possible without assumptions on plasma behavior locally (i.e. event by event). Usually, most obviously, the analysis of the measured, time series variations will involve crude estimates of large- or small-scale structures and of the degree of stationarity for each event.

[4] We apply one of these techniques below, namely the Curlometer [*Dunlop and Balogh*, 1993; *Robert and Roux*, 1993; *Robert et al.*, 1998]. Other papers [*Dunlop et al.*, 2001; *Glassmeier et al.*, 2001] explore other techniques that are relevant in some sense to the other data regimes (defined by the comparative spatial and temporal scales). The first of these deals with the application of the discontinuity analyzer [*Dunlop et al.*, 1997; *Dunlop and Woodward*, 1998, 1999]. The second addresses four spacecraft analysis in the Fourier domain, describing the first application of a number of related techniques, named the Wave Telescope [*Glassmeier et al.*, 1995; *Motschmann et al.*, 1996, 1998; *Pincon and Motschmann*, 1998].

2. Caviats of Use

2.1. Basic Definition

[5] The analysis technique applied in this paper directly combines simultaneous data across the different spacecraft to calculate the curl of the magnetic field. It uses Ampere's law to estimate the average current density through the tetrahedron formed by the spacecraft configuration, using the difference approximation

$$\mu_0 \boldsymbol{J} \cdot \left(\Delta \boldsymbol{r}_{i\wedge}\Delta \boldsymbol{r}_j\right) = \Delta \boldsymbol{B}_i \cdot \Delta \boldsymbol{r}_j - \Delta \boldsymbol{B}_j \cdot \Delta \boldsymbol{r}_i$$
$$\left\{\text{representing}: \ \mu_0 \int \boldsymbol{J} \cdot ds = \oint \boldsymbol{B} \cdot dl\right\}$$

with $\Delta \boldsymbol{r}_i \equiv \boldsymbol{r}_i - \boldsymbol{r}_1$, and similarly $\Delta \boldsymbol{B}_i \equiv \boldsymbol{B}_i - \boldsymbol{B}_1$ (see *Dunlop et al.* [1988] for a derivation). This effectively estimates the average current normal to the face (1,i,j) of the tetrahedron (see Figure 1). Since the vector defining the face is known by $\Delta \boldsymbol{r}_{i\vee}\ \Delta \boldsymbol{r}_j$, the currents normal to three faces can easily be reprojected into a Cartesian coordinate system. The fourth face

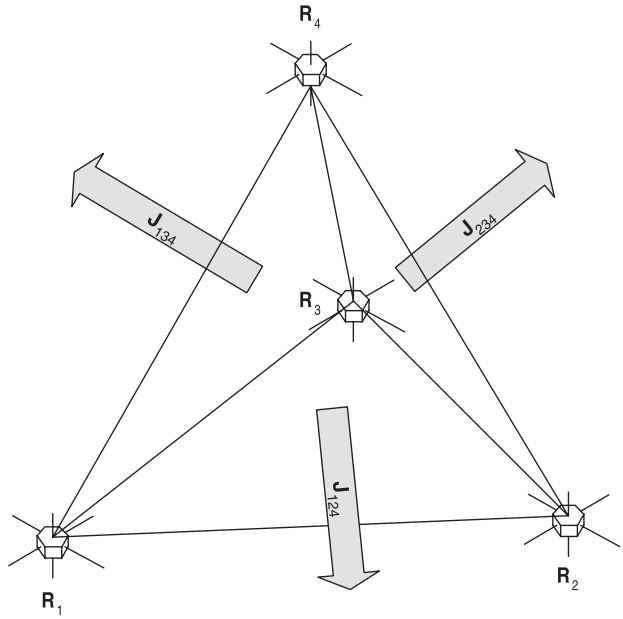

Figure 1. Illustration of the the Curlometer estimate.

gives redundant information by definition, but can be used as a consistency check on the others. A number of different formalisms now exist to calculate $\boldsymbol{J}$ (see chapters 15 and 16 of *Paschmann and Daly* [1998]) which are all mathematically identical, but which differ slightly in their application to the data (methodology). The central assumption here is a linear field variation (i.e. a linear gradient) between spacecraft so that J is constant over the spacecraft volume. Generally, this requires that the spacecraft separation is much less than the scale lengths on which the current density varies. If this assumption does not hold, the estimate of $\boldsymbol{J}$ becomes inaccurate (but may still reflect real effects). Some check on the linearity of the spatial magnetic field gradients is therefore desirable to qualify the estimate to some degree (see below).

[6] It is also possible to calculate an estimate for $div(\boldsymbol{B})$, from

$$div(\boldsymbol{B}) \mid \Delta \boldsymbol{r}_i \cdot \Delta \boldsymbol{r}_j \wedge \Delta \boldsymbol{r}_k \mid = \mid \Sigma_{cyclic} \Delta \boldsymbol{B}_i \cdot \Delta \boldsymbol{r}_j \wedge \Delta \boldsymbol{r}_k \mid$$

The calculation of $div(\boldsymbol{B})$ produces non zero values as a consequence of nonlinear spatial gradients neglected in its estimate (as well as containing the effect of timing and measurement errors, as mentioned below). It therefore usefully measures the combined effect of the linear approximation for those diagonal terms in the dyadic $\nabla \boldsymbol{B}$. The other terms in $\nabla \boldsymbol{B}$, contributing to curl($\boldsymbol{B}$), are not monitored, but for many simple current structures the nonlinear contributions to these terms can be substantially similar to those for the terms in $div(\boldsymbol{B})$ (but see below). In this sense only, $div(\boldsymbol{B})$ can provide a quality estimate for $\boldsymbol{J}_{curlometer}$ in place of the unknown error ($\boldsymbol{J}_{curlometer} - \boldsymbol{J}_{real}$), arising from the calculated, linear estimate of $\boldsymbol{J}$ (as originally noted by *Dunlop et al.* [1988]). In fact, the two quantities are often comparable in situations where the application of the Curlometer is useful (e.g. the case of simple current sheets, flux tubes or field−aligned currents).

[7] Nevertheless, each term ($div(\boldsymbol{B})$ or ($\boldsymbol{J}_{curlometer} - \boldsymbol{J}_{real}$)) is different, so that the information from $div(\boldsymbol{B})$ only

indirectly refers to the estimate of the error in $\boldsymbol{J}$. In particular, the nonlinear contributions, combine differently in each case, so that the detailed comparison of each term is somewhat sensitive to the shape and orientation of the spacecraft configuration. The use of $div(\boldsymbol{B})$ as an indicator is therefore less valid at extreme distortions of the spacecraft tetrahedron, where the orientation of $\boldsymbol{J}$ with respect to the spacecraft tetrahedron (as well as the relative anisotropies in both of these) can adversely affect the determination of $\boldsymbol{J}$. For example, at extreme anisotropy some components of $\boldsymbol{J}$ may not be well-determined, even though the overall tetrahedral scale may be small compared to the spatial gradients, and the resulting estimate of $div(\boldsymbol{B})$ may be small. At large anisotropy, either in the magnetic field or the spacecraft configuration, preferred orientations of the spacecraft tetrahedron with respect to the spatial form of the magnetic field (where the relative spatial scales and the principal tetrahedral dimensions are well matched) may, or may not, occur for a particular event. Both the shape of the spacecraft configuration and its orientation relative to the magnetic field structure are therefore important monitors to use in conjunction with the method. The former factor is known, whereas the latter depends upon some knowledge of event properties. If these properties are not known the $div(\boldsymbol{B})$ estimator can only indicate when the current estimate may be bad [*Robert et al.*, 1998], at least for the case of a regular tetrahedral configuration. Monitoring the spacecraft configuration is therefore considered to be in addition to the use of $div(\boldsymbol{B})$. We actually use the ratio $|div(\boldsymbol{B})|/|curl(\boldsymbol{B})|$ to monitor a dimensionless quantity, expressed as a percentage deviation from zero.

[8] There is also an issue of the observed time dependence, while any structure is being sampled. If $curl(\boldsymbol{B})$ is strongly time dependent, perhaps so that different fluctuations are seen at different spacecraft, depending on their location in the current layer, any estimate of the current density or $div(\boldsymbol{B})$ will be unstable. For time series measurements, observed time dependence in the measured profiles of $\boldsymbol{B}$ can either represent local temporal variations in $\boldsymbol{B}$ and $\boldsymbol{J}$, or convected motion of the spatial variations. More usually there will be a combination of both, so that coherent, high frequency variations may have different effects on the estimates of $curl(\boldsymbol{B})$ and $div(\boldsymbol{B})$ for different time resolutions. Ideally, the effective temporal gradients should be comparable with the equivalent, convected spatial gradients and this limits the usable temporal resolution of the data in each case. We will investigate this effect in future work.

[9] So far we have not mentioned the effect of measurement errors (uncertainties) in the determination of $\boldsymbol{r}$ and $\boldsymbol{B}$ (and time). These errors are very critical for the calculation of $\boldsymbol{J}$, since it involves differences in the quantities, and their contribution to the error in $\boldsymbol{J}$ is also highly sensitive to both the spacecraft configuration and the magnetic structure. *Dunlop et al.* [1990] and *Dunlop and Balogh* [1993] show that for distorted spacecraft configurations this contribution to the uncertainty in $\boldsymbol{J}$ can increase by a factor of five or more compared to that for the equivalent regular, tetrahedral configurations, for the same measurement errors ($\delta\boldsymbol{B}$, $\delta\boldsymbol{r}$). We point out here that there is a competition between the physical error in the determination of $\boldsymbol{J}$, requiring close spacecraft configurations, and measurement errors for each spacecraft in the tetrahedron. The latter, typically, become more significant at small separations (in that case, the field differences and separation vectors are small, whereas the respective errors do not reduce). There is therefore a need to reduce the absolute errors on timing, on position and on the field measurements.

[10] For all these reasons briefly referred to above, there are, of course, only some types of current systems where the method can be best applied and we illustrate these limitations in section 3. In general, the use of this technique should be supported by other analysis defining the context of the measurement, for example the region sampled (magnetospheric currents, magnetopause or tail current sheet) and character of the individual time series. Future papers will investigate the detailed application of the method, in conjunction with other analysis methods.

2.2. Testing the Curlometer With Model Fields

[11] In order to simply demonstrate the behavior of the Curlometer we use a 1-D current sheet model, in which $\boldsymbol{B}$, and hence also $\boldsymbol{J}$, vary along the x-direction only (as indicated in Figure 2). A number of explicit forms for $\boldsymbol{J}$ can be used, but here we wish to briefly illustrate the generic results. In the model there are only B_y and J_z contributions and the spacecraft tetrahedron moves along the x-direction. The size of the tetrahedron is scaled relative to the spatial scale length of the model. In Figure 3 we use model data from two different spacecraft tetrahedron configurations, and plot $div(\boldsymbol{B})$ and the 'error' in the determination of $\boldsymbol{J}$, calculated using the Curlometer technique, i.e. the magnitude of $\boldsymbol{J}_{curlometer} - \boldsymbol{J}_{model}$. Although the curves do not agree quantitatively (values have been normalized by dividing by $curl(\boldsymbol{B})$ and $\boldsymbol{J}$ respectively), the shape of the $div(\boldsymbol{B})$ curves follow those of the errors in $\boldsymbol{J}$. Thus in relative terms, $div(\boldsymbol{B})$ can provide a useful indicator of the quality of the estimate of $\boldsymbol{J}$, at least for this model and the configurations chosen. For the irregular tetrahedron, however, it is clear that $div(\boldsymbol{B})$ is poorer at matching the Curlometer error. Not all current structures have the same property, of course, and for some $div(\boldsymbol{B})$ may be a poorer indicator than for others. For real data we do not have access to the true form of $\boldsymbol{J}$, which may anyway be sampled only crudely. We use this model, therefore, as the simplest illustration of the points raised above.

[12] The error in $\boldsymbol{J}$ arises in our test from the fact that different faces of the tetrahedron sample different currents. This is because the field is nonlinear between the spacecraft and hence the linear combination of multispacecraft data in the Curlometer technique erroneously estimates the current. In fact, we can trace the origin of this error in the particular case of our model: it arises in the erroneous calculation of J_x(which is zero in the model). In the spacecraft configurations used, spacecraft 1, 2 and 3 all lie in the model xy-plane at the apices of an equilateral triangle. Thus only the sides 124 and 134 of the tetrahedron contribute to the calculation of J_x. The perpendicular bisector of the side joining spacecraft 2 and 3 is parallel to the y-axis. Spacecraft 4 lies above ($z > 0$) the xy-plane: in the first case (Figure 3a), it forms a regular tetrahedron with the other 3

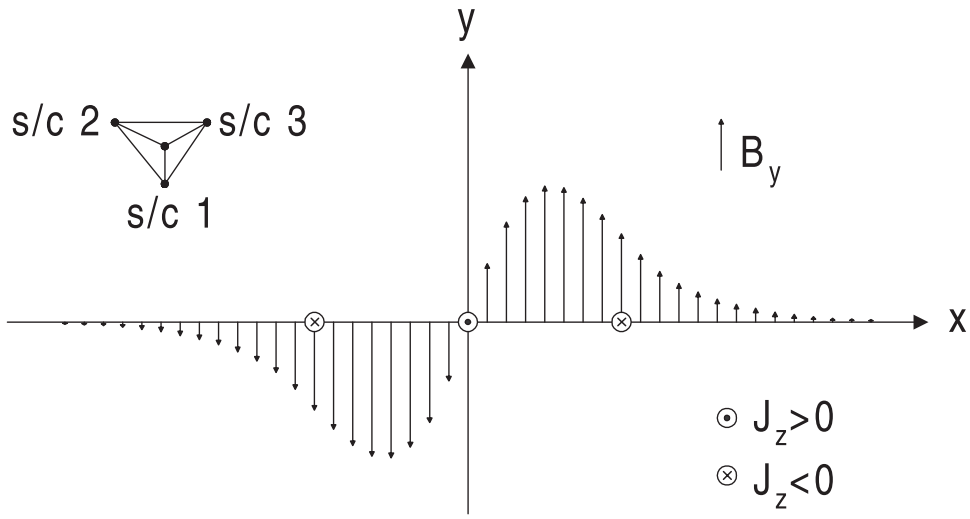

Figure 2. Schematic of the 1-D current sheet model.

spacecraft, while, in the second case (Figure 3b) it is more than five times higher than this but retains the same x and y separations from the other spacecraft. As spacecraft 4 rises in z, these faces become more perpendicular to the x-direction. Hence, the calculation of J_x becomes more accurate and the overall error in $\boldsymbol{J}$ is reduced, relative to $div(\boldsymbol{B})$.

[13] It should also be noted that $\boldsymbol{J}_{model}$ itself is not well-defined. Here we have used a simple average of the theoretical currents passing through the points of each spacecraft in the tetrahedron. However, we could also have calculated the current density at the centre of mass as an equally useful form for $\boldsymbol{J}_{model}$, for example. The conclusion to draw from this is clearly that errors on this scale are meaningless in the context of the linear assumptions on the scale of the tetrahedron.

3. Application to Selected Events

[14] For an accurate test of the Curlometer technique on real events, the magnetic field data needs to be intercalibrated to a high accuracy [see, e.g., *Khurana et al.*, 1996]; but ultimately it is uncertainties in the spacecraft position vectors, which are limiting on the accuracy of the Curlometer estimate [*Dunlop et al.*, 1990]. As a first test, therefore, we only wish to show qualitative effects and some consistency in the signatures for the estimate of $\boldsymbol{J}$, rather than making quantitative statements. We would first like to demonstrate the behavior of the method, both to highlight anomalies in the context of the discussion of section 2, and to explore the plausibility of any signatures in the magnetospheric context (such as the direction of the magnetopause or field-aligned currents). Two important points should be noted here. Firstly, not all the current signatures we discuss are real, since we wish to highlight the sampling issues discussed above, which can occur (rarely) in the relatively ordered high field region of the magnetosphere. Secondly, the issue of whether $div(\boldsymbol{B})$ performs well as a quality indicator for the estimate of $\boldsymbol{J}$ is not critical to the present demonstration: we already know that the estimates will be inaccurate (because of the

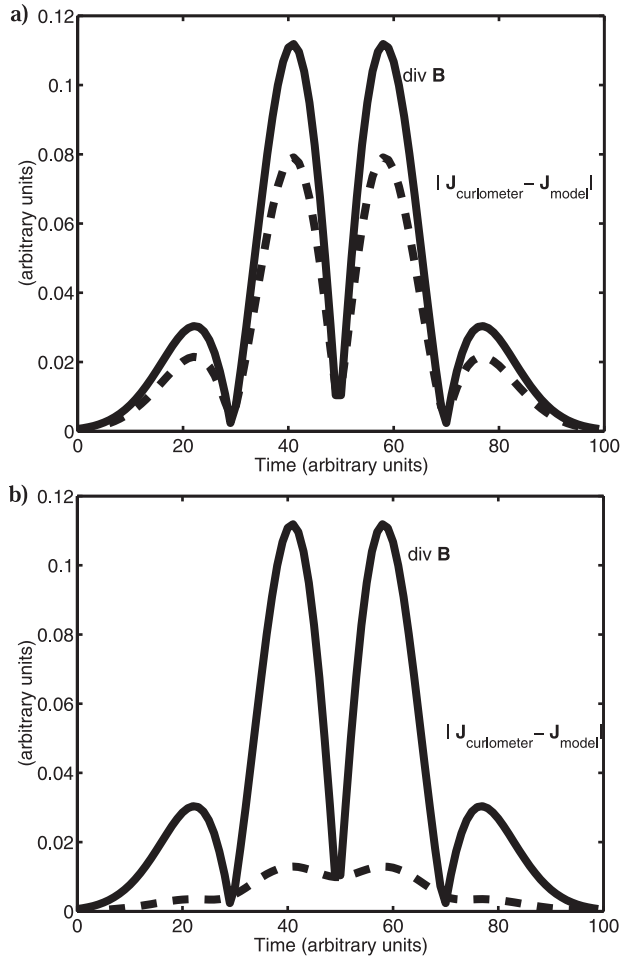

Figure 3. (a) For the left panel, $div(B)$ and $|J_{curlometer} - J_{model}|$ as calculated for a regular tetrahedron (of relative size 0.2 compared to the model scale length) flying through the current sheet model. (b) For the right panel, $div(B)$ and $|J_{curlometer} - J_{model}|$ for an irregular tetrahedron (of relative size 0.2 compared to the model scale length) flying through the current sheet model.

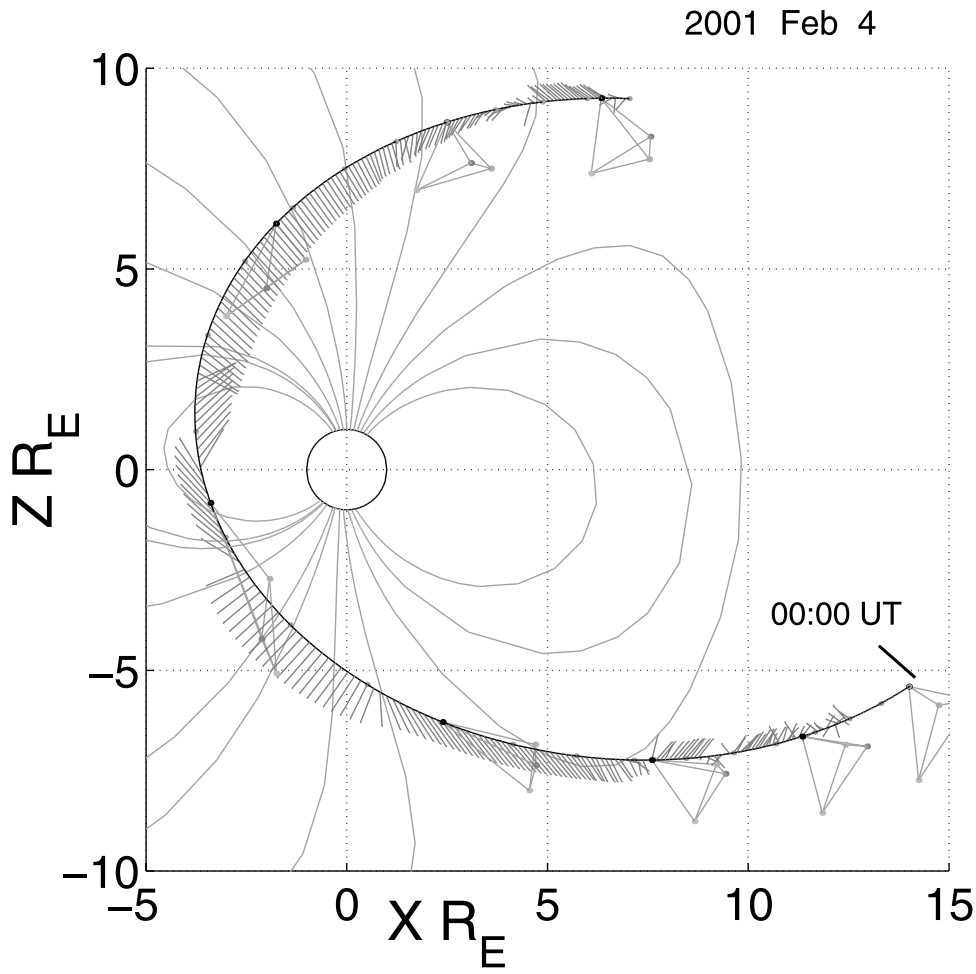

Figure 4. The Cluster orbit and configuration, shown with respect to the model field, as described in the text for 4 February 2001. The feather lines represent log measured field vectors projected into the plane.

present level of errors and the limitation on the spatial scale imposed by the Cluster configuration). Our aims in the use of these events are also to check the physical context and effect of the spacecraft configuration, and the *div*(***B***) test is monitored routinely to comment also on its behavior.

[15] In order to mask time dependent effects, as noted above in section 2, we have limited computations to a low data resolution (1–5 minutes). At high time resolutions, the estimate of *div*(***B***) is sensitive to the resolution unless events are carefully chosen. This effect needs further investigation, but it is clear that at Cluster separations, which generally can be of the order of the scale size of any boundary layer containing currents, each spacecraft can sample distinct plasma regions. For example, at the magnetopause, one or more spacecraft may be in the highly variable magnetosheath while the others are within the magnetospheric boundary. We will include the analysis at higher resolutions in future work.

3.1. Anomalous Behavior in Quiet Fields

[16] As a first illustration, we analyse the data taken on the 4 February 2001. The orbit and spacecraft configuration for the whole of this day is shown in Figure 4. Here, the orbit from spacecraft 1 is shown, together with the configuration of the other spacecraft at particular, simultaneous times around the orbit. The configuration represents the set of spacecraft separation vectors, giving relative positions at each time. In Figure 4 the configuration has been scaled by a factor of 20. The positions of each spacecraft are coloured as follows: spacecraft 1 (black), spacecraft 2 (red), spacecraft 3 (green), spacecraft 4 (magenta). Figure 4 also shows model field lines [*Tsyganenko*, 1989] for guidance. Also indicated is a feather plot along the orbit of the projected, measured field components (spacecraft 1), as logarithmic values, which can be seen to follow the model field (in direction) at most positions. The spacecraft are inbound on the southern leg of the orbit, pass through perigee, and then exit the magnetosphere through the northern leg of the orbit. This pass was chosen because the magnetic activity level within the magnetosphere was extremely quiet ($Kp = 1$) and allowed a close sampling of the background, high magnetospheric field ($>50-100\ nT$) to be made, together with significant comparison to the Tsyganenko, T89 model magnetic field [*Tsyganenko*, 1989]. The configurations show significant distortion through perigee and in fact the configuration near 16:40 UT is near planar in shape. Since the measured field shows smooth variations, we might expect that any trends in the computed estimate of *curl*(***B***) to be affected primarily by the spacecraft configuration for

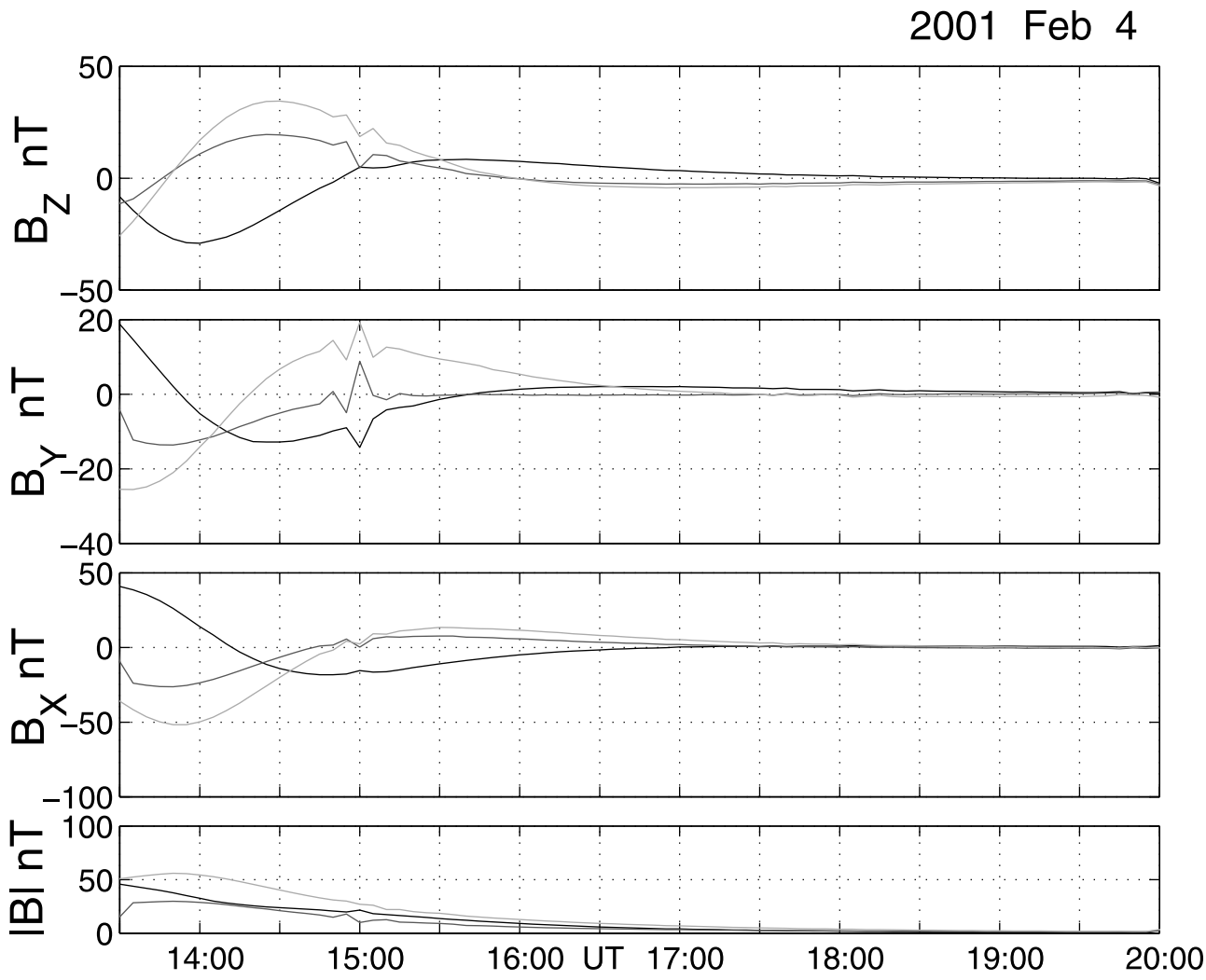

Figure 5. Field differences between each spacecraft pair (referenced to spacecraft 3) for the high field interval on 4 February 2001, in GSE components.

that segment of the orbit. There ought to be little or no actual current contained in the T89 model in this region, outside the ring current and tail current sheet and this is confirmed by computing the small-scale gradients along the given orbit of spacecraft 1.

[17] It is instructive to look first at the differences in the magnetic field vectors between each pair of spacecraft. From 08:15–13:30 UT there was a data gap for spacecraft 3, however, so that in Figure 5 we show the field differences for the outbound pass from 13:30 UT (all referenced to spacecraft 3), which corresponds to positions just after perigee. It is apparent that these differences are changing direction as the northern part of the magnetosphere is traversed. This reflects the evolution of the spacecraft configuration with respect to the magnetic field, which is changing its relative orientation (as well as its shape). There is at least one significant perturbation in the background field at 15:00 UT, probably associated with a traversal through field lines mapping to the polar cap boundary, but we do not study this feature in detail here (see below).

[18] Figures 6a and 6b show the computed GSE components of the Curlometer estimate of $\boldsymbol{J}$ and $div(\boldsymbol{B})$ for both the model, T89 field (K_P = 1) and the actual data in the same format. The bottom panels are different: for the model this is the estimated $|\boldsymbol{J}|$ and for Cluster data it shows where there are data gaps. The feature around 16:40 UT is associated with the collapse of the spacecraft tetrahedron into a planar configuration, as referred to above, and does not represent a real current, but rather the result of the distorted configuration magnifying the contribution to the calculation of $curl(\boldsymbol{B})$ from the sources of error, including the approximation of the gradients (see discussion in section 2). Nevertheless, the model calculation and the data show very similar trends in this calculation of $curl(\boldsymbol{B})$. The estimates in each case are therefore consistent with each other (the sampling of the Tsyganenko model at these spacecraft separations (~600 km) is similar to the data). Thus, with real data, the method is behaving as predicted (if anomalously), but is known to be a bad estimate in this case. The larger values contained in Figure 6b reflect both the fact that the measured field does show different values from the model field, and that there are implicit errors in the actual positions and field values (which also have magnified contributions to $curl(\boldsymbol{B})$). The field model has been sampled at the given orbital positions so contains only errors due to the linear approximation on the scale of the Cluster config-

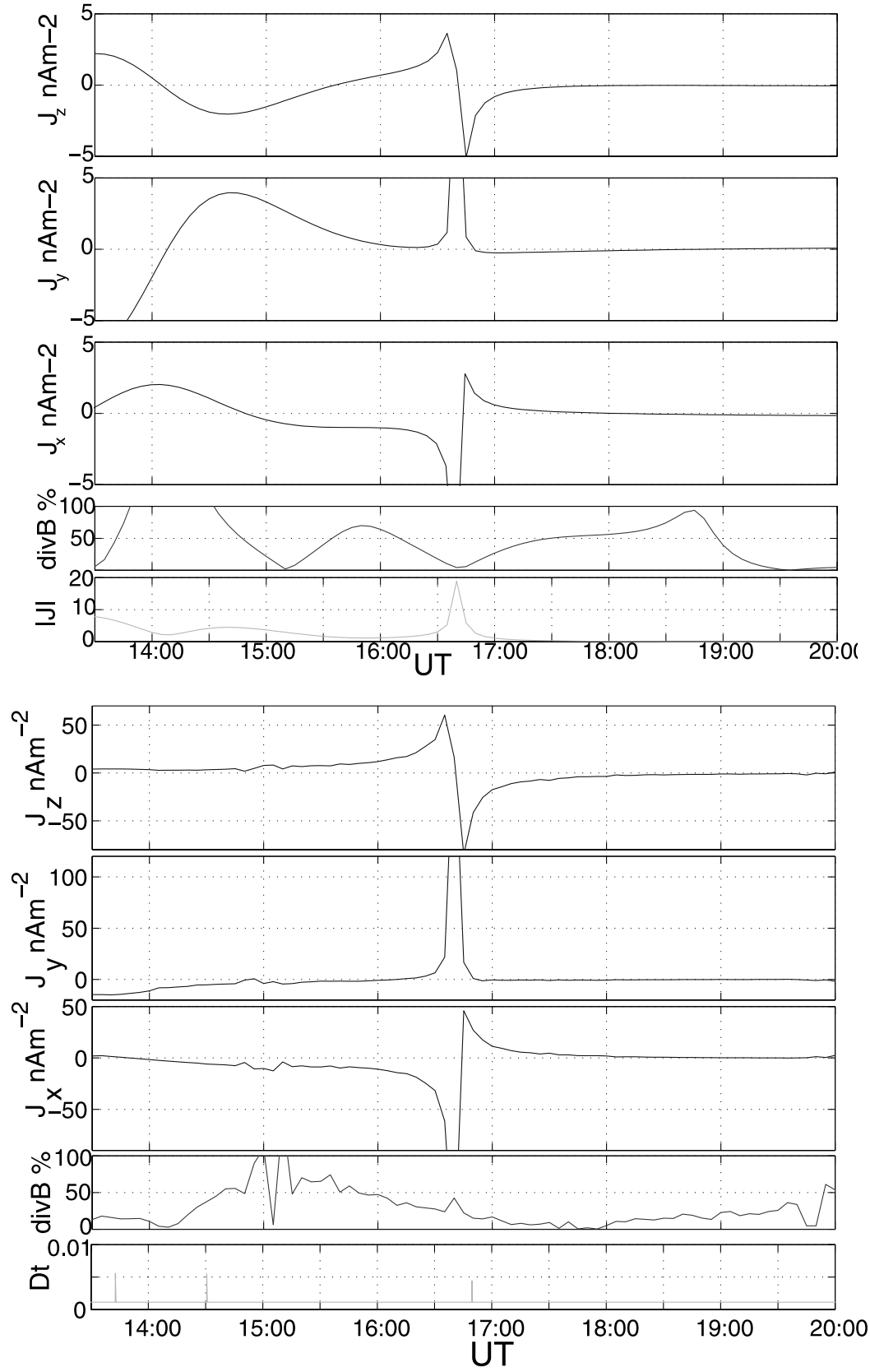

Figure 6. (a) The computation of the Curlometer current estimate of the T89 model field, for the spacecraft configuration on the 4 February 2001, as described in the text. Since spacecraft positions are given directly to the model, there are only sampling errors due to variation of the current over the spacecraft volume. (b) Similar plot as for Figure 6a, but calculated for actual data. Since the field sampled is real, both positional uncertainty and measurement errors can contribute to the Curlometer calculation.

uration. Measurement errors on $\boldsymbol{B}$ in fact are relatively unimportant above ~50 nT (even preliminary calibrations are likely to be less than 1% in this regime) and at these Cluster separations the error on position, $\boldsymbol{r}$, is ~1%. However, the large amplification of the error contributions to *curl*($\boldsymbol{B}$) at the extreme distortion of the tetrahedron are significant. We find that a 0.1 nT and a 1 km error contributes somewhat less than half of the difference in magnitude between the model and the data.

[19] Figure 6b shows in addition, some small amplitude variations (in $|\boldsymbol{J}|$), particularly the feature observed at 15:00 UT, which could be associated with a field-aligned current (aligned to the background field to within ~20°), although the signature is only marginally significant. For instance, it is apparent that in this region the value of the *div*($\boldsymbol{B}$) ratio remains below 50%, except for the period around 15:00 UT, although there are differences in the profiles for the model and for those in the data. At the extreme spacecraft configuration at 16:40 UT, however, we do not expect that div($\boldsymbol{B}$) will remain a good quality indicator and the bottom panel in Figure 6a in fact shows that the low value of div($\boldsymbol{B}$)/|curl($\boldsymbol{B}$)| is a result of the large anomalous value of |curl($\boldsymbol{B}$)| at that time. The high value of div($\boldsymbol{B}$) at the current perturbation seen around 15:00 UT is consistent with this feature being poorly resolved.

3.2. Identification of Currents at Low Field Magnitude

[20] In contrast to the quiet, high field situation, Figure 7 shows the inbound, low field interval and corresponds to magnetosheath data until the high latitude, magnetopause (southern cusp) crossing at 07:15 UT. Figure 7a shows four spacecraft magnetic field data at the resolution of the Curlometer estimate, which is shown in Figure 7b in the format of Figure 6b. The dashed vertical lines correspond to significant bursts of large $\boldsymbol{J}$ at times when *div*($\boldsymbol{B}$) remains below 50% and there are no highly distorted configurations during this interval. Just after 07:15 UT, the magnetopause is associated with a large increase in $\boldsymbol{J}$ to over 50×10^{-9} Am^{-2}. The direction of this current is not in $+Y_{GSE}$, but the magnetospheric field direction suggests the magnetopause crossing lies just south, and within, the exterior cusp region so we expect this is representative of a current within the cusp, where a strong J_y is not expected. Instead the current appears to be directed across the cusp throat. The other times correspond to magnetosheath features and for most of the large bursts of estimated current, div($\boldsymbol{B}$) remains small. The fact that the cusp current is plausible gives some confidence that these magnetosheath currents reflect real structures. The times for which the div($\boldsymbol{B}$) ratio is greater than 50% all correspond to small amplitude values of current.

[21] Figure 8 shows similar, low field data at the magnetopause, corresponding to 10 November 2000 (as discussed by *Dunlop et al.* [2001]). The spacecraft are again inbound on the southern leg of the orbit, but now on the dusk flank magnetopause at ~19 UT. The vertical lines now indicate selected, large bursts of current. The two inner lines correspond to boundary layer encounters, where the spacecraft lie either side of the magnetopause. The value of div($\boldsymbol{B}$) does not remain small throughout the duration of these bursts. The scale size of the magnetopause layer was estimated by *Dunlop et al.* [2002] to be ~1000 km, with the current layer less than half this thickness. In both these examples, therefore, the magnetopause current sheet is thinner than the spacecraft separation and it is expected that *div*($\boldsymbol{B}$) will be significant and that the estimate of $\boldsymbol{J}$ will be inaccurate. Nevertheless we expect and find $\boldsymbol{J}$ to be directed approximately in the direction obtained here. The first of the two inner lines, at ~4:35 UT, corresponds to a fairly clean magnetopause crossing and in fact is directed southward and duskward, consistent with this location on the magnetopause. The second current increase, at 05:30–50 UT, exhibits large $-Z_{GSE}$ and $-Y_{GSE}$ components (i.e., the Y component is reversed). In fact, this time corresponds to an interval when the spacecraft had entered the magnetopause boundary layer, with some spacecraft dipping in and out of the magnetosheath. A number of magnetosheath and magnetospheric FTE signatures were observed, indicating that reconnection of flux is occurring, perhaps locally. Such FTE signatures would be expected to affect the direction of the observed magnetopause current, and this is what we find. There is a further, very fast magnetopause crossing at 6:30 UT, which is too short to be resolved on this scale (both in time and on the scale of the spacecraft configuration). The fact that the estimate of div($\boldsymbol{B}$) increases in excess of 100% at this time, is consistent with this view and indicates that an unresolved feature is present (i.e. that the calculated values of $\boldsymbol{J}$ are poorly estimated at that time). The other bursts in $\boldsymbol{J}$ are marked by the two outer lines and are again magnetosheath features, which we don't discuss in detail here.

3.3. Identification of Magnetospheric Currents at High Activity

[22] Figure 9 shows a contrasting example, on the 31 March 2001 which occurred following the intense solar storm and CME arrival at the Earth on this and the previous day, when activity levels were measured at $K_P = 9+$. Figure 9a shows a plot of the four spacecraft magnetic field, at spin resolution (4s), where the spacecraft are outbound from perigee in order to show fully the magnitude of the magnetic fluctuations within the magnetosphere. The spacecraft exit the magnetosphere near and north (tailward) of the northern cusp in a manner similar to 4 February 2001, but slightly dawnward of the presumed cusp location. Figure 9b shows the corresponding plot for the Curlometer estimate. In addition, the corresponding values obtained from the T89 model are overplotted in green and show that the model current estimates are in this case insignificant compared to the actual measured currents. Thus, nearly all the signatures in the data are due to externally induced currents on this day. The vertical dashed lines correspond to the largest features. The first pair of lines, at 8:15 UT and 8:45 UT, appear to correspond to a pair of oppositely directed, field-aligned currents (FACs), given the background field direction at these times, which is aligned to within 15° of the current bursts. The third feature, at 10:15 UT, is associated with a large value of div($\boldsymbol{B}$), and so is probably not accurate. The last feature corresponds to the magnetopause exit at 11:40 UT and produces a small value for div($\boldsymbol{B}$). The direction of this current is northward, dawnward and anti-sunward, as expected for this high latitude location, and lies parallel to the magnetopause boundary.

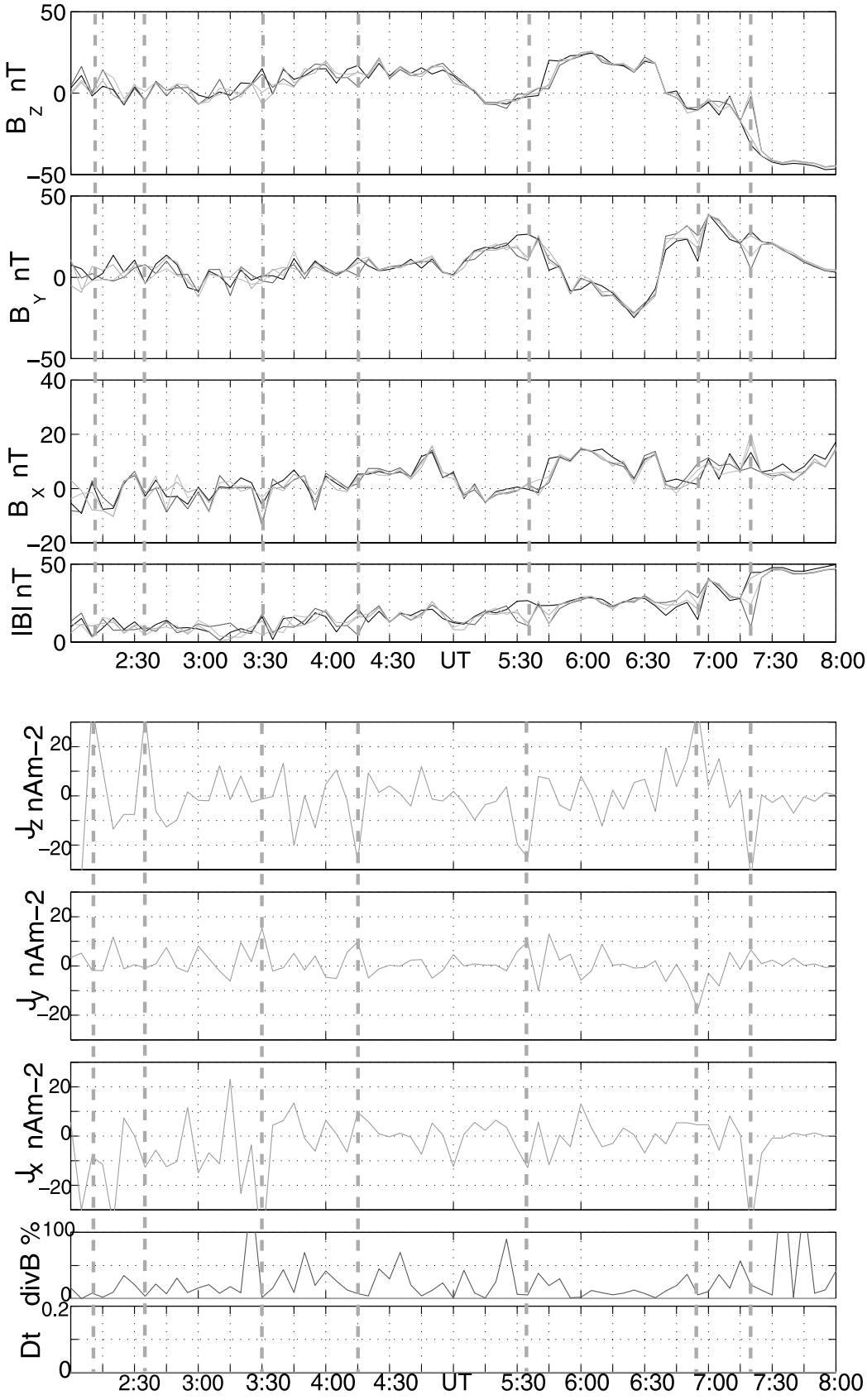

Figure 7. (a) Low time resolution plot of the magnetic field, in GSE components, for the low field interval, as described in the text. (b) Curlometer estimate for the same period as for Figure 7a, in the same format as Figure 6b and as described in the text.

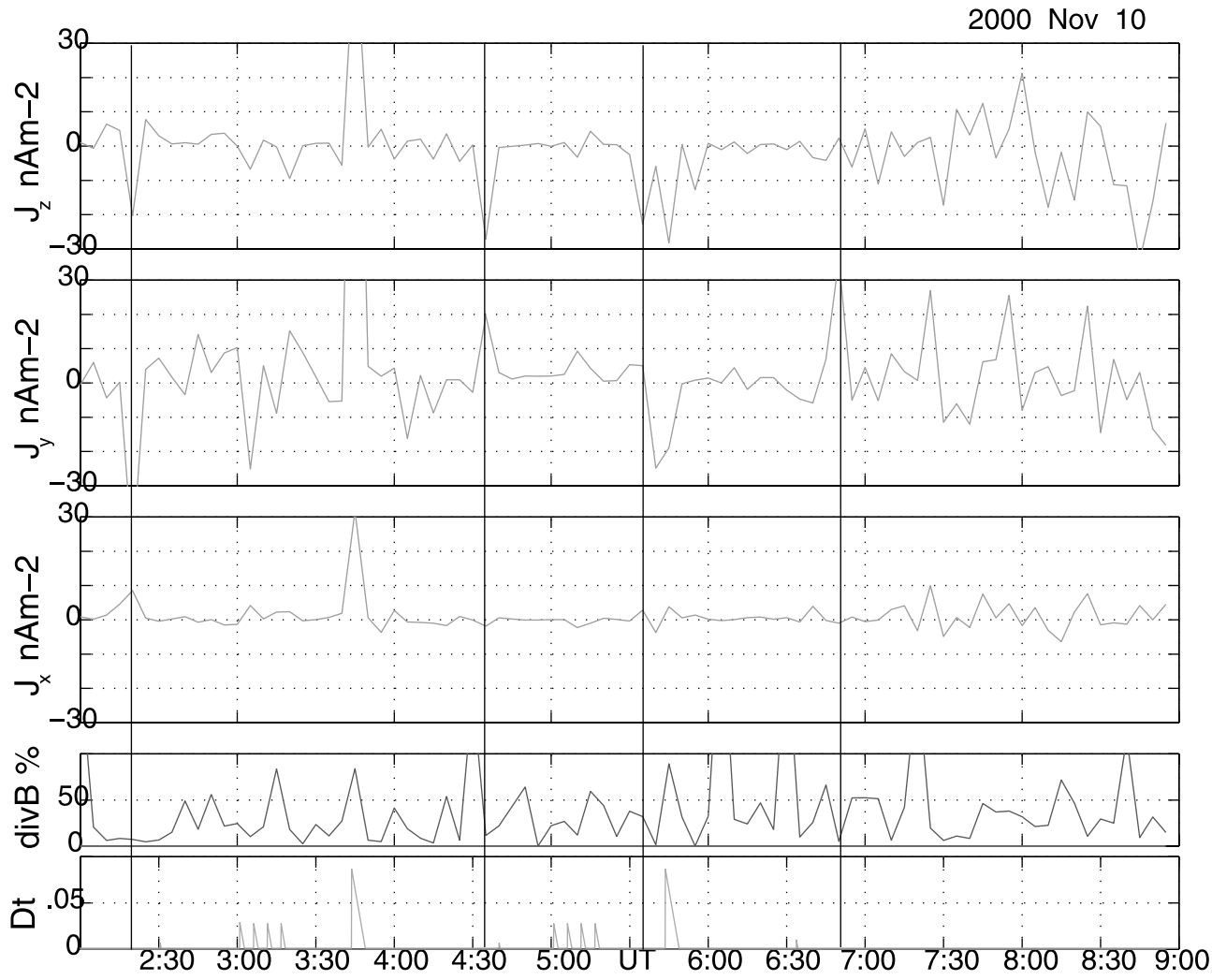

Figure 8. Similar plot as for Figure 7b, but for the 10 November 2000 and as described in the text.

3.4. Identification of Dayside Magnetopause and Boundary Layer Currents

[23] The final example we take is another set of magnetopause crossings, in the vicinity of the northern cusp, observed during an outbound pass on 26 January 2001, as shown in Figure 10. The data and Curlometer estimate are shown in Figure 11 as before. The spacecraft are located on the duskside, but approximately level with the cusp location on the magnetopause. Figure 10 shows that the magnetospheric field orientation is followed reasonably closely during the outbound pass, bearing in mind that the orbit is located duskward of noon. Figure 11a shows that the spacecraft appear to exit through the magnetospheric lobe, on tailward field lines (B_z −ve and B_x, initially, +ve). The initial crossing of the magnetopause is at ∼9:15 UT, and corresponds to a brief exit into the magnetosheath and return into the dayside boundary (possibly entry layer, near the cusp). Later, the magnetopause is crossed several times between ∼10:30 and 11:05 UT. The corresponding Curlometer plot in Figure 11b shows that there are bursts of current at each of the crossings and that in nearly all cases the direction of the magnetopause current is maintained, showing a very stable signature. This direction (northward, dawnward and tailward) is consistent with the inferred location of the spacecraft relative to the cusp. It is significant that between these series of magnetopause crossings, and for the brief crossing at ∼9:15 UT, the value of div(***B***) remains very low (fluctuating up to ∼15%). This gives us confidence that the current direction, at least, accurately reflects the real value. The importance of this last example lies in the fact that at each crossing the current bursts are similar, which could reflect a stable magnetopause current. Anomalous values depend on the sampling of the field and so are unlikely to give the same current at each encounter.

[24] Following this series of crossings there is also an isolated, and very clear, FTE signature in the magnetosheath at ∼11:32 UT. Although there is a small signature in the Curlometer estimate at this time, the current profile is not clear at this resolution. A detailed study of the current through the associated current tube will be the subject of future work (A. Roux et al., private communication, 2001).

4. Conclusion

[25] We have applied the Curlometer technique to actual four-spacecraft Cluster data for the first time and have

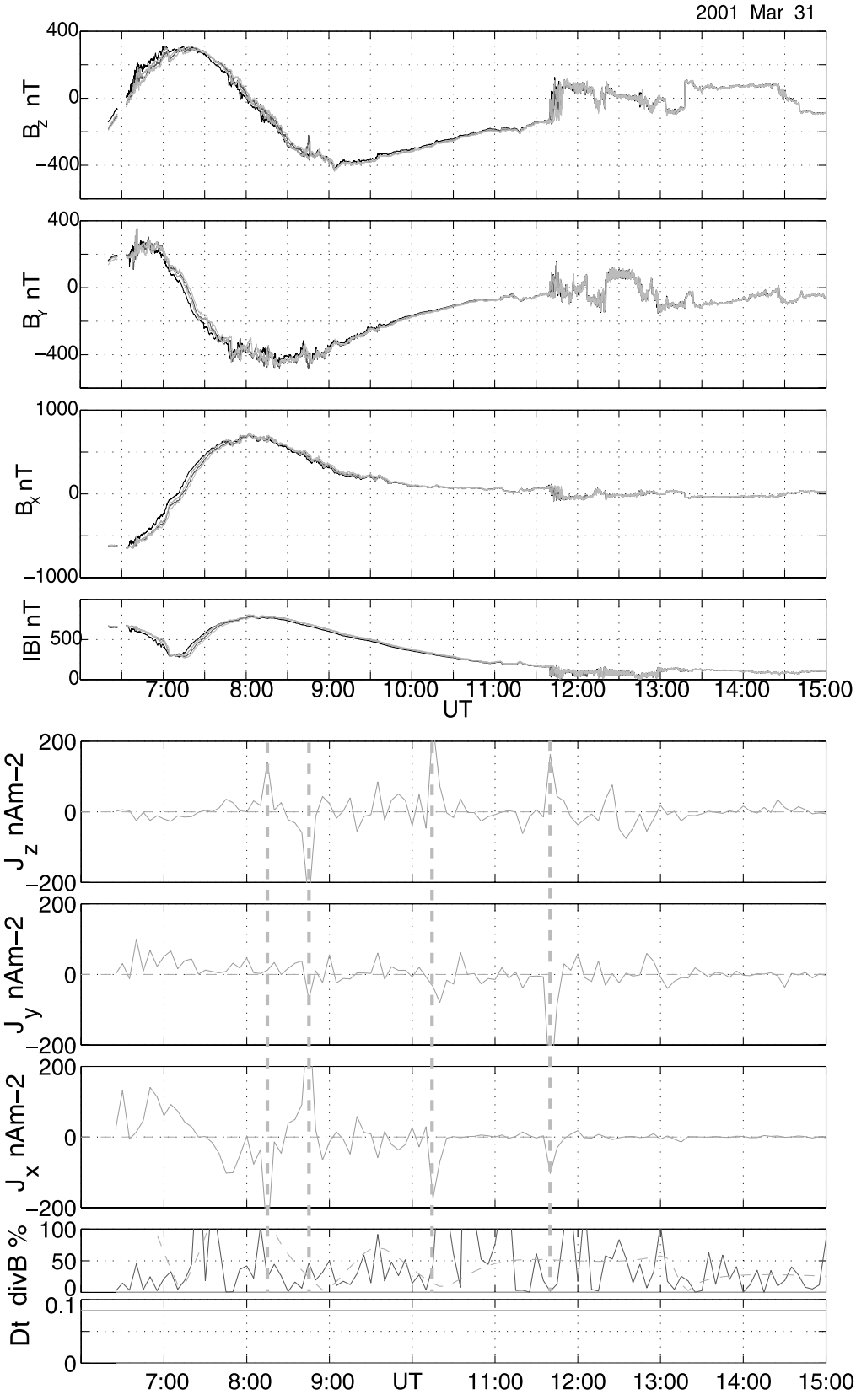

Figure 9. (a) Spin resolution magnetic field data for the 31 March 2001 (b) The corresponding computation for the Curlometer estimate, as described in the text.

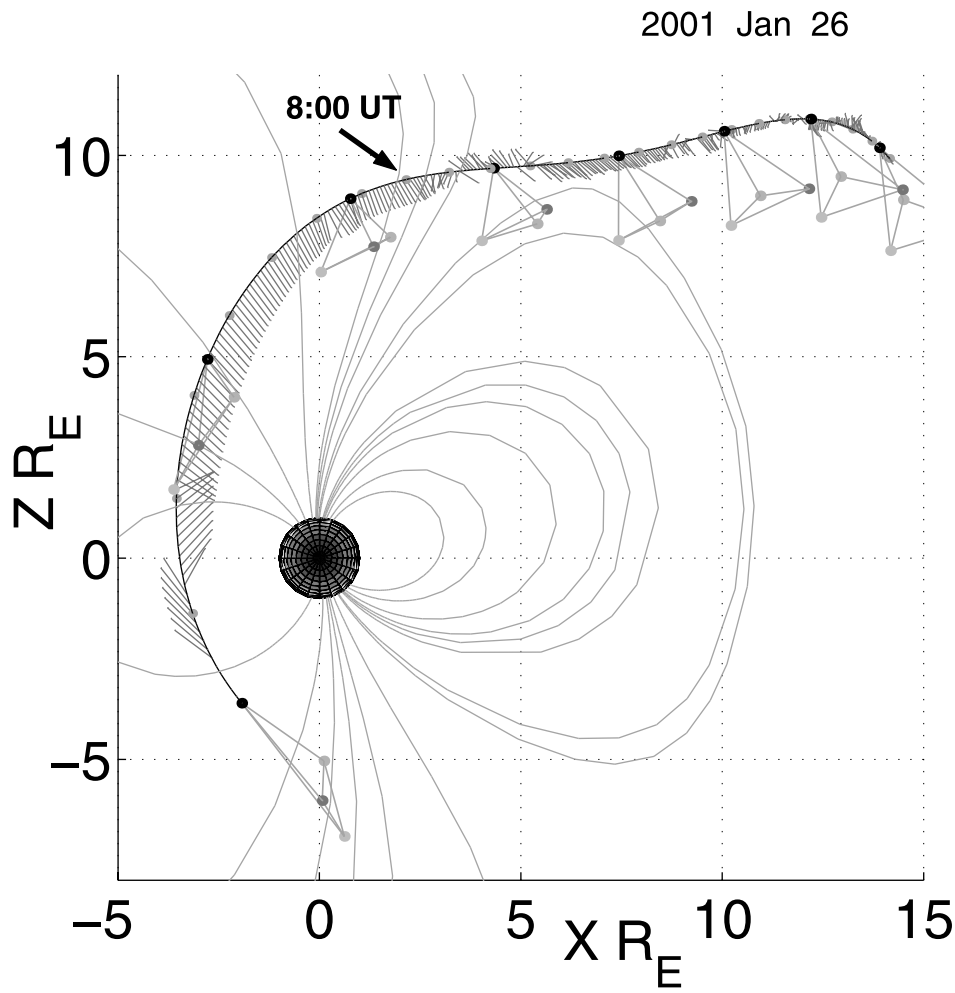

Figure 10. Similar plot as for Figure 4, but for the 26 January 2001 and as described in the text.

concentrated only on a demonstration of its operation here. The method is applicable (best suited) to a particular data regime (depending on the size of the spacecraft separations and the event scale length(s)). There are therefore a number of caveats of use, which we have referred to in the discussion and have attempted to explore by selection of a number of examples of use. These caveats relate to the basic assumptions about the ability to separate spatial and temporal variations mixed in the time series data, limitations arising from the approximation of spatial and temporal structure imposed by the Cluster array and contributions from the basic measurement uncertainties. The Curlometer is mainly sensitive to measurement errors and to the spatial sampling achieved. This can be demonstrated in a controlled way within those high field regions of the magnetosphere lying outside regions of significant current density. We have shown that for a particularly quiet pass, the application of the Curlometer to actual data follows, at least in trend, the estimate obtained from the T89 model during extreme distortions of the spacecraft configuration. The estimate produces an anomalous current, primarily as a result of the large contributions from all error sources at these extreme distortions.

[26] Even at low time resolution, the Curlometer method nevertheless produces understandable results in a number of cases, reflecting current structure in a plausible (if inaccurate) way. At high activity within the magnetosphere we identify field-aligned currents, probably associated with the polar cap boundary, and in low field regions at the magnetopause we identify magnetopause currents, consistent with each spacecraft location. In addition a number of magnetosheath current sheets are resolved. The cusp currents are also significant, and plausible. During an interval containing multiple crossings of the magnetopause, the Curlometer gave a sequence of stable current directions, consistent with the expected magnetopause current, together with an extremely low value of div($\boldsymbol{B}$). These two features together leave little doubt that the Curlometer estimate is valid in those cases and is an example of use where the physical context is clear.

[27] In effect, for application of the Curlometer assumptions are made during event selection, since it is apparent

Figure 11. (opposite) (a) Spin resolution magnetic field data for the 26 January 2001 (b) The corresponding computation for the Curlometer estimate, as described in the text.

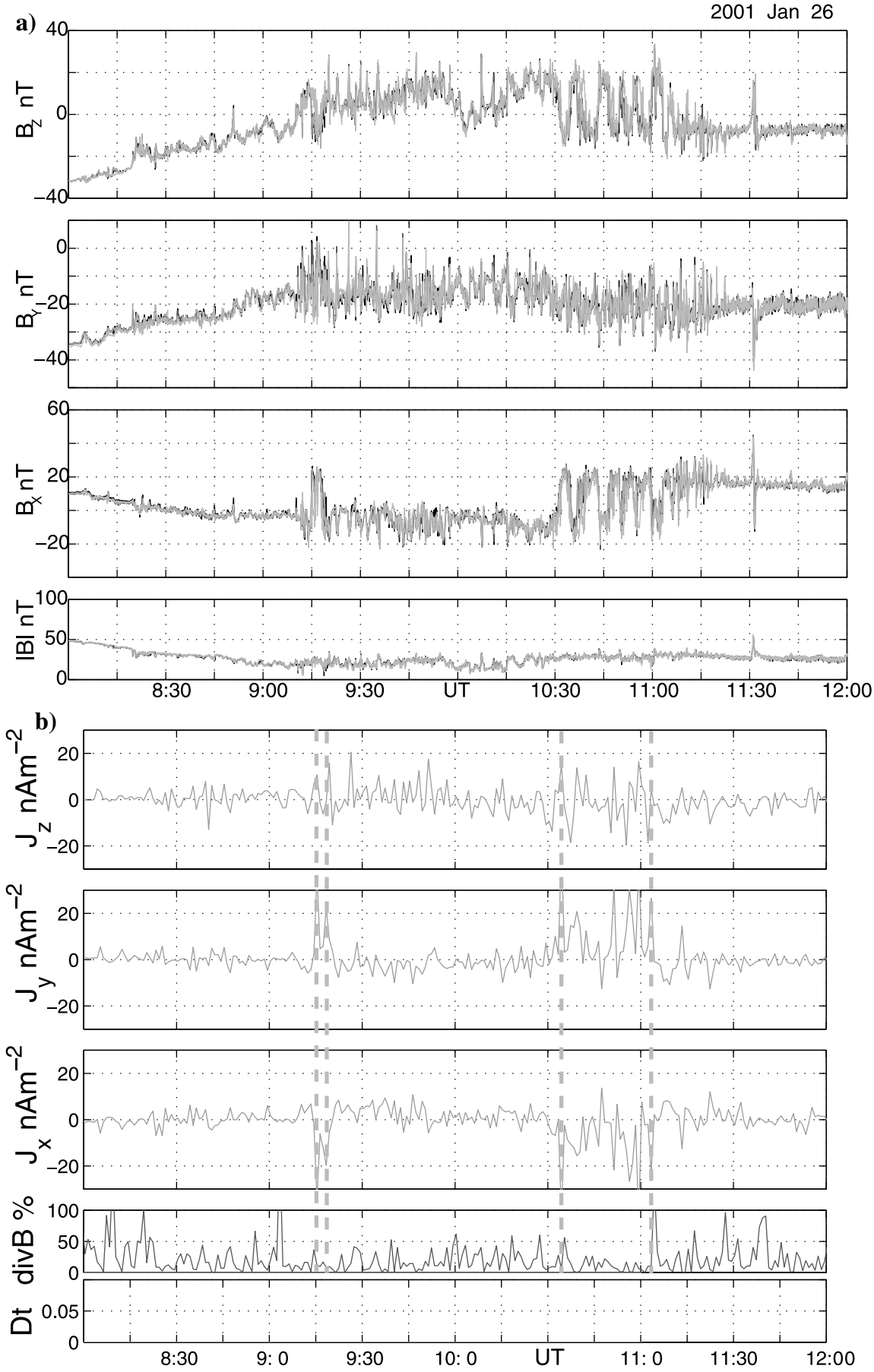

that the method can be in error in the cases described above. There is some indication that temporal variations appear to affect the practical operation of the Curlometer more critically than originally envisaged because the presence of high frequency variations in the high time resolution measurements can produce large values of $div(\boldsymbol{B})$. This statement will be investigated in future work. In this regard it is possible that the ideal events are those for which the temporal variations are equivalent to the effective convected spatial scales and this too will be investigated. Furthermore, a major test of the Curlometer result, not available when the present work was performed, will be the comparison with both the ion and electron velocities, as well as the computation of $\boldsymbol{J}_{\vee}\boldsymbol{B}$, and other derived quantities.

[28] **Acknowledgments.** This work was supported by PPARC. Michel Blanc thanks Charles Farrugia and another referee for their assistance in evaluating this paper.

References

Balogh, A., et al., The Cluster Magnetic Field Investigation: Overview of in-flight performance and initial results, *Ann. Geophys.*, *19*, 1207, 2001.

Dunlop, M. W., and A. Balogh, On the analysis and interpretation of four spacecraft magnetic field measurements in terms of small scale plasma processes, in *Spatio-temporal Aanalysis for Resolving Plasma Turbulence* (*START*), *Eur. Space Agency WPP, ESA WPP-047*, 223, 1993.

Dunlop, M. W., and T. I. Woodward, Discontinuity analysis: Orientation and motion, in *Analysis Methods for Multispacecraft Data*, *ISSI Sci. Rep. SR-001*, p. 271, Kluwer Acad., Norwell, Mass., 1998.

Dunlop, M. W., and T. I. Woodward, Analysis of thick, non-planar boundaries using the discontinuity analyser, *Ann. Geophys.*, *17*(8), 984, 1999.

Dunlop, M. W., D. J. Southwood, K.-H. Glassmeier, and F. M. Neubauer, Analysis of multipoint magnetometer data, *Adv. Space Res.*, *8*, 273, 1988.

Dunlop, M. W., A. Balogh, D. J. Southwood, R. C. Elphic, K.-H. Glassmeier, and F. M. Neubauer, Configurational sensitivity of multipoint magnetic field measurements, in *Proceedings of the International Workshop on Space Plasma Physics Investigations by Cluster and Regatta*, *Eur. Space Agency Spec. Publ., 1990. ESA SP-306*, 23, 1990.

Dunlop, M. W., D. J. Southwood, and A. Balogh, The Cluster configuration and the directional dependence of coherence lengths in the magnetosheath, in *Proceedings of Spatio-Temporal Analysis for Resolving Plasma Turbulence* (*START*), *Eur. Space Agency WPP, ESA WPP-47*, 295, 1993.

Dunlop, M. W., T. I. Woodward, D. J. Southwood, K.-H. Glassmeier, and R. C. Elphic, Merging 4 spacecraft data: Concepts used for analysing discontinuities, *Adv. Space Res.*, *20*, 1101, 1997.

Dunlop, M. W., A. Balogh, P. Cargill, R. C. Elphic, K.-H. Fornacon, E. Georgescu, and F. Sedgemore-Schultess, Cluster observes the Earth's magnetopause: Co-ordinated four-point measurements, *Ann. Geophys.*, *19*, 1449, 2001.

Dunlop, M. W., A. Balogh, and K.-H. Glassmeier, Four-point Cluster application of magnetic field analysis tools: The discontinuity analyzer, *J. Geophys. Res.*, *107*, doi:10.1029/2001JA005089, in press, 2002.

Glassmeier, K.-H., and F. M. Neubauer, Analysis of multipoint magnetometer data, *Adv. Space Res.*, *8*(9), 273, 1988.

Glassmeier, K.-H., U. Motschmann, and R. R. von Stein, Mode recognition of MHD wave fields at incomplete dispersion measurements, *Ann. Geophys.*, *13*, 76, 1995.

Glassmeier, K.-H., et al., Cluster as a wave telescope: First results from the Fluxgate Magnetometer, *Ann. Geophys.*, *19*, 1439, 2001.

Khurana, K. K., E. L. Kepko, M. G. Kivelson, and R. C. Elphic, Accurate determination of magnetic field gradients, *IEEE Trans. Magn.*, *32*, 5193, 1996.

Motschmann, U., T. I. Woodward, K.-H. Glassmeier, D. J. Southwood, and J.-L. Pincon, Wavelength and directional filtering by magnetic measurements at satellite arrays: Generalized minimum variance analysis, *J. Geophys. Res.*, *101*, 4961, 1996.

Motschmann, U., K.-H. Glassmeier, and J.-L. Pincon, Multi-spacecraft filtering: Plasma mode recognition, in *Analysis Methods for Multispacecraft Data*, *ISSI Sci. Rep. SR-001*, p. 79, Kluwer Acad., Norwell, Mass., 1998.

Neubauer, F. M., and K.-H. Glassmeier, Use of an array of satellites as a wave telescope, *J. Geophys. Res.*, *95*, 19,115, 1990.

Paschmann, G., , and P. Daly (Eds.), *Analysis Methods for Multispacecraft Data*, *ISSI Sci. Rep. SR-001*, Kluwer Acad., Norwell, Mass., 1998.

Pincon, J.-L., and U. Motschmann, Multi-spacecraft filtering: General framework, in *Analysis Methods for Multispacecraft Data*, *ISSI Sci. Rep. SR-001*, p. 65, Kluwer Acad., Norwell, Mass., 1998.

Robert, P., and A. Roux, Accuracy of the estimate of J via multi-point measurements, in *Proceedings of the International Workshop on Space Plasma Physics Investigations by Cluster and Regatta*, *Eur. Space Agency Spec. Publ., 1990. ESA SP-306*, 51, 1990.

Robert, P., and A. Roux, Dependence of the shape of the tetrahedron on the accuracy of the estimate of the current density, in *Spatio-temporal Analysis for Resolving Plasma Turbulence* (*START*), *Eur. Space Agency WPP, ESA WPP-047*, 289, 1993.

Robert, P., M. W. Dunlop, A. Roux, and G. Chanteur, Accuracy of current density determination, in *Analysis Methods for Multispacecraft Data*, *ISSI Sci. Rep., SR-001*, Kluwer Acad., Norwell, Mass., 1998.

Sonnerup, B. U. O., and M. Scheible, Maximum and minimum variance analysis, in *Analysis Methods for Multispacecraft Data*, *ISSI Sci. Rep., SR-001*, p. 185, Kluwer Acad., Norwell, Mass., 1998.

Tsyganenko, N. A., A magnetospheric field model with a warped tail current sheet, *Planet. Space Sci.*, *37*(1), 5, 1989.

A. Balogh, Space and Atmospheric Physics Group, Imperial College, London, SW7 2BZ, UK. (m.dunlop@ic.ac.uk)

M. W. Dunlop, Space Sciences Division, SSTD, Rutherford Appleton Laboratory, Chilton, Didcot, Oxfordshire OX11 0QX, UK. (m.dunlop@rl.ac.uk)

K.-H. Glassmeier, Institut für Geophysik und Meteorologie, TUB, 38106 Braunschweig, Germany.

P. Robert, CETP/IPSL, 10–12 Avenue de l'Europe, 78140 Velizy, France.